

This is a repository copy of *Probing carbon black deagglomeration in lithium-ion battery cathode manufacturing using powder resistivity metrics*.

White Rose Research Online URL for this paper: <a href="https://eprints.whiterose.ac.uk/id/eprint/232802/">https://eprints.whiterose.ac.uk/id/eprint/232802/</a>

Version: Published Version

### Article:

Lian, G.J. orcid.org/0009-0000-0753-7917, Verma, P., Cumming, D. orcid.org/0000-0003-1923-2250 et al. (1 more author) (2025) Probing carbon black deagglomeration in lithiumion battery cathode manufacturing using powder resistivity metrics. Journal of Power Sources, 659. 238311. ISSN: 0378-7753

https://doi.org/10.1016/j.jpowsour.2025.238311

### Reuse

This article is distributed under the terms of the Creative Commons Attribution-NonCommercial-NoDerivs (CC BY-NC-ND) licence. This licence only allows you to download this work and share it with others as long as you credit the authors, but you can't change the article in any way or use it commercially. More information and the full terms of the licence here: https://creativecommons.org/licenses/

### Takedown

If you consider content in White Rose Research Online to be in breach of UK law, please notify us by emailing eprints@whiterose.ac.uk including the URL of the record and the reason for the withdrawal request.



ELSEVIER

Contents lists available at ScienceDirect

# Journal of Power Sources

journal homepage: www.elsevier.com/locate/jpowsour





# Probing carbon black deagglomeration in lithium-ion battery cathode manufacturing using powder resistivity metrics

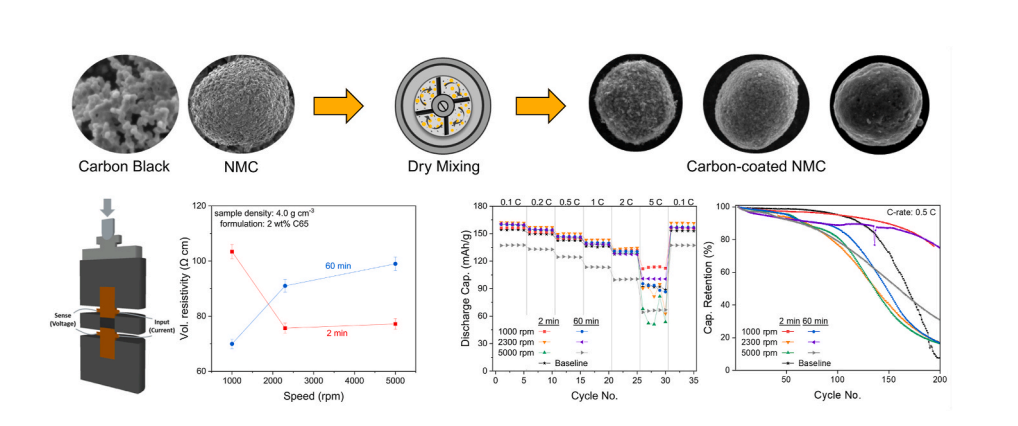
Guo J. Lian <sup>a</sup>, Prateek Verma b, Denis Cumming a,c,\*, Rachel M. Smith a,c

- a Department of Chemical and Biological Engineering, University of Sheffield, Mappin Street, Sheffield, S1 3JD, United Kingdom
- <sup>b</sup> School of Chemical and Process Engineering, University of Leeds, Woodhouse, Leeds, LS2 9JT, United Kingdom
- <sup>c</sup> The Faraday Institution, Quad One, Harwell Science and Innovation Campus, Didcot, OX11 0RA, United Kingdom

#### HIGHLIGHTS

- Powder resistivity provides a mechanistic proxy for carbon black deagglomeration.
- Dry mixing conditions dictate carbon coating and free carbon structures.
- Carbon coating extent alters both electronic and ionic transport properties.
- Balanced coating and free carbon structures improve cell performance.
- Tailored carbon coatings improve rate capability and cycling stability of electrodes.

#### GRAPHICAL ABSTRACT



### ARTICLE INFO

Keywords:
Dry mixing
Conductive additive
Carbon black deagglomeration
Electronic conduction
Carbon coating

### ABSTRACT

Carbon black dispersion is critical to achieving a percolated network in lithium-ion battery electrodes. Existing knowledge relies on legacy insights, lacks mechanistic understanding, and direct quantification of dispersion remains challenging due to nanoscale particle sizes. This study presents the first mechanistic investigation of carbon black deagglomeration via mechanofusion, using powder resistivity to examine deagglomeration behaviour, linking dry mixing parameters, CBD structures and coating characteristics. Low powder resistivity can be achieved with a short mixing time, while optimal mixing speed depends on carbon loading and mixing time. Inadequate mixing results in inhomogeneous distribution of conductive additives, and excessive mixing breaks down large carbon black structures necessary for long-range conduction, increasing powder resistivity. While powder resistivity correlates with deagglomeration, it does not directly predict electrochemical performance. These findings highlight the importance of a combination of long and short-range contacts in the carbon binder domain, facilitated by conductive carbon coatings, to enhance electrochemical performance. This work introduces a practical technique to assess carbon black deagglomeration, traditionally evaluated through slurry, electrode, or cell-level properties. Powder resistivity can be effectively used to correlate carbon black structures

<sup>\*</sup> Corresponding author. Department of Chemical and Biological Engineering, University of Sheffield, Mappin Street, Sheffield, S1 3JD, United Kingdom. E-mail address: d.cumming@sheffield.ac.uk (D. Cumming).

#### 1. Introduction

Lithium-ion battery (LIB) electrodes are composites with a complex structure obtained by a slurry consisting of active material, conductive additive, and polymeric binder in a solvent, coated onto a current collector. Cathode active materials generally have lower electrical conductivity compared to the anode. For example, NMC has a conductivity of  $10^{-6} - 10^{-2}$  S cm<sup>-1</sup> [1] depending on composition, and decreases with increasing lithium content, while graphite, a common anode material, has a conductivity of  $\sim 10^4$  S cm<sup>-1</sup> [2]. Additionally, the polymeric binder is electrically insulating. The addition of conductive additives is crucial not only for the formation of the carbon binder domain (CBD) but also for increasing the point-to-point electrical contact of active materials for electrical conduction. The CBD also influences the pore networks and systems for ionic conduction. Therefore, the CBD structures can greatly impact the electrochemical performance of cathodes. Electrode heterogeneity greatly affects rate capability, where a non-uniform distribution of active material and conductive additive can lead to uneven electrode porosity and thickness [3-5]. It was shown that a carbon-rich layer near the current collector improved rate capability by up to 20 % [3]. Targeted CBD distribution localised next to active material particles enhances conduction [6]. Additionally, processing techniques with different mixing mechanisms greatly influence CBD formation and the resulting electronic and ionic networks [7]. The extent to which conductive additives are broken down governs long-range conduction, while processing intensity and contact intimacy dictate the short-range contacts [8].

In conventional wet slurry mixing, the extent of mixing and distribution of the active material, conductive additive, and binder is often unknown and unmeasured [9]. Challenges arise when attempting to spatially design the distribution of conductive additives and, specifically, the balance between long and short-range electrical contacts. This is particularly important for micron-sized NMC and nano-conductive carbon systems. A comprehensive review of electrode structures and electronic conductivity was reported by Entwistle et al. [8]. Current thinking defines these two pathway lengths vaguely based on their length scale [7–10]. Long-range electronic pathways can be categorised as the conventional understanding of electronic conduction, where the interconnected network spans between the active material particles within the 0.1–10 μm range. These form interconnected pathways that span across the entire electrode, from active material particles to the current collector. Short-range electronic contacts involve the nearest neighbouring interactions between active material particles and adjacent CBD or particles, typically within the 1-100 nm length scale. Baumgärtner et al. [9] further discussed the concept of a medium-range pathway through the active material, differentiating from the short-range pathway that solely represents the interfacial resistance.

In our previous work [11,12], we proposed two CBD structures influencing electronic conductivity in LIB cathodes: (1) bridge structures occupying the spaces between NMC particles and forming the contact points between two particles; and (2) film structures covering the surface of NMC particles. The bridge structure correlates to the long-range electronic pathways that form a percolated electrical network within electrodes. The film structure correlates to the short-range contacts, acting as interparticle electrical contact points to facilitate electronic conduction between active material particles and the neighbouring CBD. Subsequent calendering could further increase contact between these CBD structures to enhance electrode performance [13,14]. The film structure is analogous to carbon coatings established through wet or dry routes, as demonstrated in various publications [15–18]. The primary concern is uncontrolled film formation arising from the non-uniform

dispersion of carbon black in wet slurry mixing. This can lead to a decrease in the effective interface between active material particles and electrolyte. Therefore, it is important to control carbon black dispersion through a mechanistic approach to tailor the desired film structure.

Carbon black dispersion also affects the electronic conduction mechanisms within lithium-ion battery cathodes. The percolation theory describes how electronic conductivity of a binary mixture of a certain material and conductive additives changes as a function of the conductive additive content (Fig. 1) [19]. Other mechanisms include quantum mechanical tunnelling, where electrons that are excited and possess higher kinetic and potential energies can jump over potential barrier gaps [20]. In carbon black aggregates, electrons move along the connected aggregate pathways until contact is made with another aggregate [21,22]. Similarly, for primary particles, conduction also relies on particle, though tunnelling can also occur [21,23]. Although these mechanisms are widely accepted across different applications [9, 20,24–26], differentiating, and quantifying these different conduction mechanisms remains extremely challenging, especially within the complex CBD matrix.

Recent publications investigating the quantification of carbon black deagglomeration were carried out through particle size analysis [27–30], slurry rheological properties [6,28], or electrode and CBD structures [27,29,31] correlated with electrochemical performance. The process is time-consuming and requires significant experimental effort for slurry preparation or electrochemical testing before any indications of dispersion can be determined. Additionally, some techniques, such as those involving slurry properties, are not suited for dry electrode processing, where the distribution of the conductive additives and binder

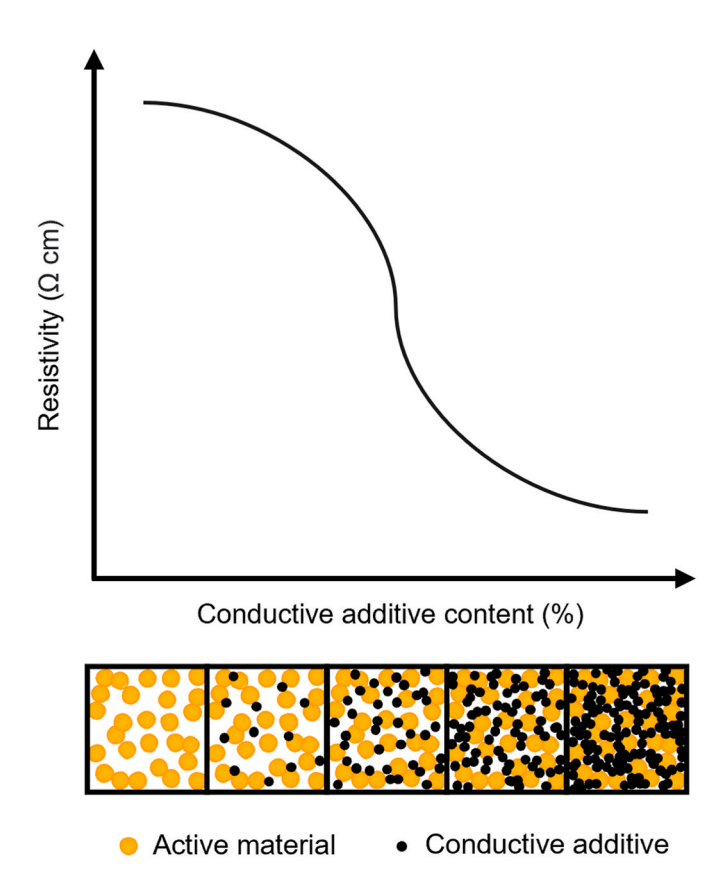


Fig. 1. Percolation curve depicting the change in resistivity with increasing conductive additive content. Adapted from Ref. [8]. CC by 4.0.

remains an important aspect. Various powder characterisation methods employed include: (1) volume resistivity measurements, where deagglomeration can be correlated to bulk resistivity in binary powder mixtures [32]; (2) bulk and tapped density measurements where deagglomeration results in a better packing [33]; (3) particle size distribution where deagglomeration causes shift in distribution peaks [27,30].

This study demonstrates volume resistivity as a promising proxy for further investigation of carbon black deagglomeration behaviour during mechanofusion mixing. While widely used to evaluate conductive additive suitability [32,34,35], measurements can be affected by contact resistances and experimental variation [36]. Improved setups, such as a guard-electrode method [37] and silver-coated probes [38] have been developed to improve accuracy. In a binary powder mixture of cathode active material and conductive additives, resistivity depends on the conductive additive content. Deagglomeration of carbon black agglomerates into smaller constituents disrupts the interconnected "chain-like" structures that enable continuous electronic pathways, thus affecting bulk resistivity.

Here, mechanofusion approaches were systematically extended to control carbon black deagglomeration during the dry mixing of NMC622 and carbon black. We demonstrated the application of a conventional resistivity measurement technique to probe carbon black deagglomeration. Particle surface morphology and process parameters were analysed to understand the impact of carbon black structures on active material electronic conductivity. Electrochemical performance of the electrodes demonstrated that the structure of the conductive network is altered by carbon coatings, which strongly influences rate capability and cycling stability. The insights obtained from this study provide valuable guidance for the pre-processing of active material for wet slurry mixing and aid in advancements of dry electrode processing.

### 2. Materials and methods

### 2.1. Materials

Commercially utilised NMC622 (LiNi $_{0.6}$ Mn $_{0.2}$ Co $_{0.2}$ O $_{0.2}$ ) from BASF SE (d $_{50}=11.1~\mu m$ , density = 4.74 g cm $^{-3}$ , theoretical capacity = 175 mAh g $^{-1}$  at 4.2 V cut-off voltage) was used as the cathode active material. The conductive additive used was carbon black C-NERGY<sup>TM</sup> Super C65 from Imerys (d $_{50}=32~nm$ , density = 1.60 g cm $^{-3}$ ). The polymeric binder was poly(vinylidene) fluoride (Solvay Solef® 5130) from Sigma Aldrich. The solvent for slurry preparation was N-methyl-2-pyrrolidone (NMP) from Sigma Aldrich (99.5 % purity). All materials were used as received.

### 2.2. Experimental method

Binary powder mixtures of NMC622 and C65 were prepared in a Nobilta  $^{\rm TM}$  Mini (Hosokawa Micron Corp.) mixer with varying NMC622: C65 wt% formulations. All mixtures were weighed accordingly, making up a total of 20 ( $\pm 0.1$ ) g for each sample. The mixer was then rotated to a horizontal orientation. The powder mixture was first pre-mixed at 500 rpm for 2 min to disperse and homogenise the binary powder mixture and then mixed for up to 60 min at 1000/2300/5000 rpm (tip speed = 4.61/10.6/23.04 m s $^{-1}$  respectively). The clearance between the rotor blade and the inner wall of the mixing chamber was 1 mm. The temperature of the mixer (average range of 19–22 °C) was regulated using a cooling water source and air flow was maintained at approximately 2.8 L min $^{-1}$ .

The binary powder mixtures were used to prepare the slurry for NMC622 electrodes based on the formulation of 96:2:2 wt% NMC:C65: PVDF using a Thinky mixer (Intertronics). The prepared slurry was coated onto an aluminium foil (thickness  $=15~\mu m$ ) using a draw down table (MSK-AFA-L800-H110, MTI Corp.) with a doctor blade gap of 150  $\mu m$ . The coated film was dried at 80 °C for 1 h under ambient atmosphere. The dried electrodes ( $\sim\!50~\%$  porosity) were calendered to  $\sim\!40~\%$  porosity using a hot roller machine (MSK-HRP-01, MTI Corp.) at

 $80\,$  °C. Slurry formulations and electrode properties are provided in Tables S1 and S2 respectively.

2032 stainless steel (316SS) coin half-cells were assembled using a 0.5 mm 316SS spacer,  $\varnothing$  14.8 mm calendered NMC electrode as the cathode, a  $\varnothing$  15 mm lithium metal chip (thickness = 250  $\mu m$ , areal capacity =  $\sim\!50$  mAh cm $^{-2}$ ) as the counter electrode, a  $\varnothing$  16 mm glass microfibre GF/F filter (GE Whatman, thickness =  $\sim\!420~\mu m$ ) as the separator, a 1 mm 316SS spacer, and a 316SS wave spring. 90  $\mu L$  of 1 M LiPF $_6$  in an ethylene carbonate (EC) and ethyl methyl carbonate (EMC) (30:70 wt% EC:EMC) solvent with 2 wt% vinylene carbonate was used as the electrolyte (Sigma-Aldrich).

### 2.3. Characterisation

A field emission gun scanning electron microscope (FEG-SEM) (Inspect F50, FEI Company) was used to examine the surface morphology of carbon-coated NMC622 particles. Samples were prepared by attaching loose powders to conductive carbon tape attached to an aluminium stub. Compressed air was blown from the edge of the carbon tape to remove excess powder for better imaging. Samples were coated with gold using a sputter coater prior to imaging.

The electrical volume resistivity of the powder samples was measured using the 2-probe method through a 4-wire in-house designed compression jig, as shown in Fig. 2. The set-up consists of an insulating mould (material: Nylon 66) with a  $\emptyset$  12 mm die. The moulds were supported by two copper contact stamps from both ends, each attached to two insulated cables, connected to a digital multimeter (DMM7510, Keithley Instruments). The mould with contact stamps was fitted into a load frame (LF10CONF0001-P) equipped with a 10 kN load cell (TX00723) from GDS Instruments where precise compression load was applied. Contact stamps on both ends were each connected to the INPUT (current) terminals and SENSE (voltage) terminals on the multimeter. The 4W- $\Omega$  configuration was used with the "offset compensation" setting enabled. Contact stamps were cleaned and polished as required to minimise the interfacial contact resistance between the copper stamps and the sample.

To carry out resistivity measurements, several grams of sample were weighed and filled into the die. As samples consist of different carbon loading, free carbon content and varying carbon black structures, powder packing can vary significantly. Since the die has a fixed volume, the remaining unfilled sample was then weighed and used to determine the total sample mass filled into the die. A separate contact stamp was used to apply pre-compaction by hand to ensure as much sample was fitted into the die as possible. Next, an initial compaction force of 50 N was applied under the load frame, and the initial height of the powder sample was measured using a standard digital height gauge. All measurements were carried out at room temperature (approximately 20 °C). starting by applying a load of 100 N, with further increments of 100 N, up to 2000 N. Resistance values at corresponding compression forces were recorded after a 1 min stabilisation period after the force was applied. The corresponding height of the powder sample was measured using a 10 mm linear displacement transducer kit with an accuracy of 0.07 % FRO (GDS Instruments).

The electrical volume resistivity  $(\varphi)$  at the corresponding powder density  $(\rho)$  were calculated using Equations (1) and (2) based on the methodology reported by Spahr et al., as shown below [32]. The volume resistivity is denoted by the symbol  $\sigma$  by Spahr et al., but here, it is denoted by the symbol  $\varphi$  to avoid confusion with the conventional symbol of  $\sigma$  for electronic conductivity.

$$\varphi = R \frac{A}{h} \tag{1}$$

$$\rho = \frac{m}{Ah} \tag{2}$$

where R is the measured electrical resistance, A is the cross-sectional

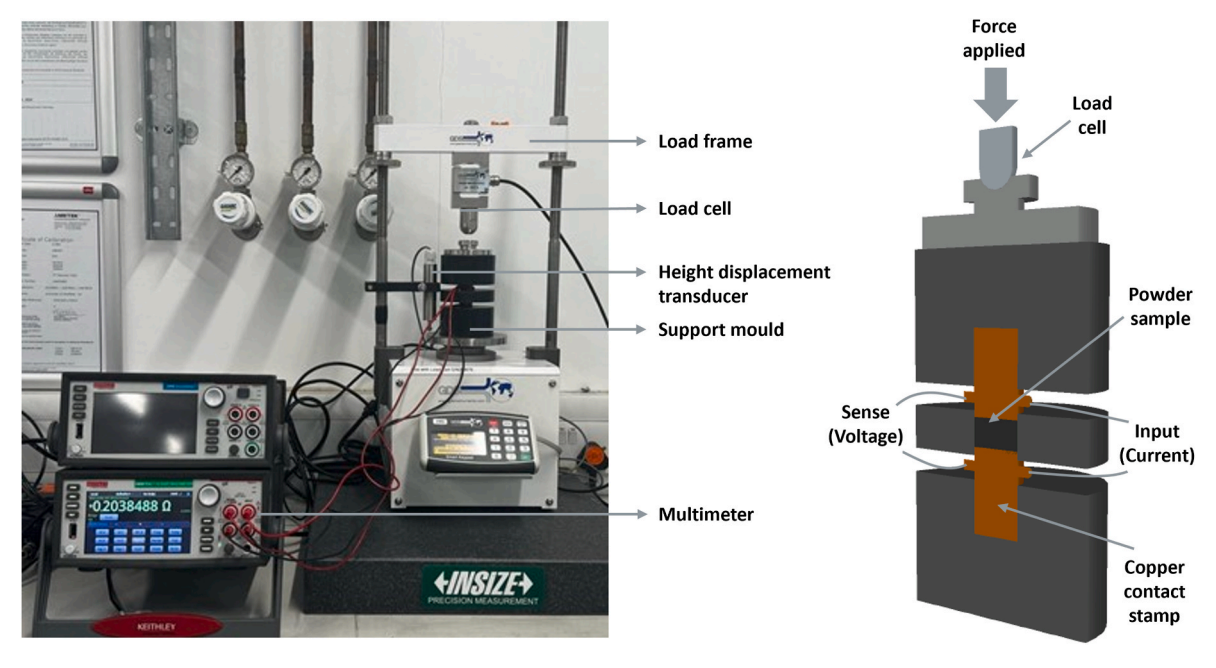


Fig. 2. Setup of the in-house designed compression jig used for resistivity by compression measurements (left) and schematic showing the compression support mould (right).

area of the die, h is the sample height and m is the sample mass.

The galvanostatic charging and discharging cycling of coin cells was performed at different C-rates between the voltages of 3.0–4.2 V using a Maccor 4000 Automated Test System under a temperature of 25  $^{\circ}\text{C}.$ 

#### 3. Results and discussion

### 3.1. Surface morphology of coated particles

The surface morphology of polycrystalline NMC622 particles resembles a framboidal (blackberry-like) texture formed by the aggregates of the crystallites (Fig. 3a). The grains of these crystallite aggregates form "pores" or "grooves" on the surface of the NMC secondary particle. The structure of these grooves is important as they increase the area of

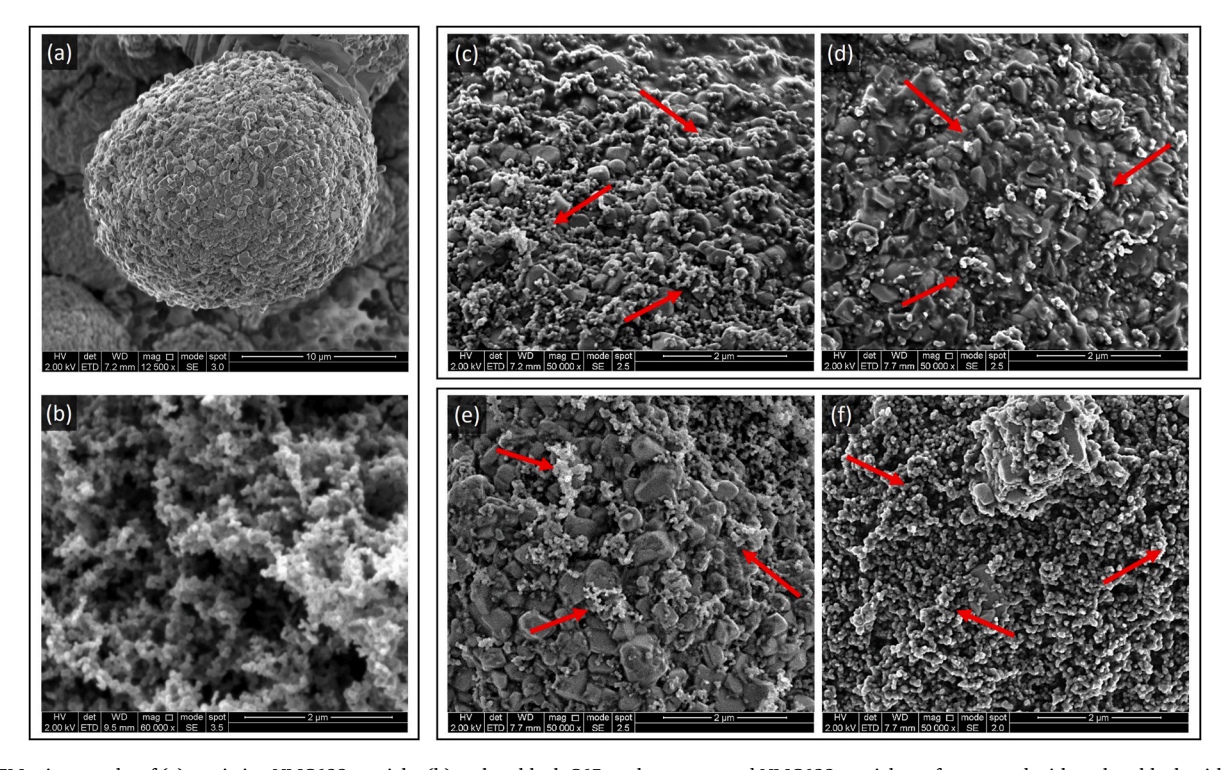


Fig. 3. SEM micrographs of (a) a pristine NMC622 particle, (b) carbon black C65 agglomerates and NMC622 particle surface coated with carbon black with C65 wt% and mixing time of (c) 2 wt% 2 min, (d) 2 wt% 60 min, (e) 10 wt% 2 min and (f) 10 wt% 60 min.

contact of the NMC particles with the CBD. The CBD is the cluster of conductive additive and polymeric binder formed during slurry mixing and is crucial to forming a percolated electronic pathway. From a manufacturing point of view, the carbon black-polymer clusters impart gel-like characteristics to form a rheologically stable slurry [39]. The pores on the NMC622 surface can also increase particle surface area in contact with the electrolyte to enhance ionic conduction [40].

Carbon black, shown in Fig. 3b, is generally small colloidal particles with a primary particle size of 10-100 nm and low bulk density [41] compared to cathode active materials. Due to the small primary particle size, carbon black particles experience interparticle interactions through van der Waals forces, giving rise to the formation of larger aggregates or agglomerates. These aggregates or agglomerates are in the size ranges of ~100 nm to a few microns and can affect dispersibility and electronic conductivity [42]. This is in contrast with the active material particles where the average size is 11.1 µm. Previous studies have shown that nano-sized carbon black can occupy the voids between micron-sized NMC particles, forming conductive networks to enhance electron transfer within the electrode microstructure [8,9,12,32]. When two carbon black particles come together, both attractive and repulsive forces increase with different respective magnitudes. The resultant force response curve indicates that a maximum attraction is reached at the minimum of the potential well. Carbon black particles that are trapped in this potential well form agglomerates. To separate them, by moving out of this potential well, energy input is required. Therefore, it is critical to consider the breakdown of these agglomerates into smaller constituents to promote dispersion within NMC particles to improve electronic contacts.

Carbon black deagglomeration can be separated into two steps: rupture and erosion [30,35]. Rupture is the abrupt breakage of agglomerates into aggregates once a critical shear stress is achieved. This is related to the energy required to overcome the van der Waals forces between primary particles that hold them together to form the agglomerates. Erosion refers to the further deagglomeration of aggregates, resulting in a decreased aggregate size or reduction into primary particles. This process occurs at a lower shear stress over a longer period of time, so larger aggregates are gradually reduced to smaller aggregates or primary particles. This dispersion behaviour is observed when NMC is mixed with C65 through mechanofusion, and presumably, rupture occurs immediately when mixing starts, provided the critical shear stress has been reached based on the process conditions. Simultaneously, during mechanofusion, carbon black is attached to the NMC surface due to continued compression, progressively forming a coating around the NMC particle. Further mixing results in a coating consisting of very small aggregates or primary particles, where the erosion process continues, followed by compaction of the coating and spheronisation of the surface, resulting in a smooth carbon-coated NMC particle. Dispersion of carbon black is well-studied in industrial rubber applications, and dispersibility remains the same point of focus in battery manufacturing [43]. Weber et al. suggested that the erosion process is influenced by carbon black properties, specifically slower erosion with increasing specific surface area [30]. As deagglomeration is a result of energy input, dictated by process parameters, it is possible to control the extent of deagglomeration and coating to tailor the desired film structures for active materials.

SEM micrographs in Fig. 3c–f show that the varying carbon black structures (indicated by red arrows) on NMC particles after mixing are closely linked to the rupture and erosion process. Carbon blacks are clustered, aggregated structures made up of small, spherical particles and appear as a slightly brighter contrast. The background, consisting of granular-shaped particles, corresponds to the crystallite aggregates of NMC and appears as a slightly darker contrast.

For a short mixing time of 2 min, carbon black attached to NMC were mainly agglomerates or large aggregates regardless of carbon loading (Fig. 3c and e). The main difference between the two samples is the size of the carbon black structures. At higher carbon loading, carbon black

structures appeared larger and less evenly distributed (Fig. 3e), indicating that the deagglomeration process was less efficient within the same mixing period. This can be attributed to the constant overall energy input being distributed across a greater number of agglomerates, thereby reducing the specific shear stress acting on individual agglomerates. Consequently, the applied shear stress likely did not exceed the critical threshold needed to overcome the van der Waals forces holding the primary particles together. As such, the rupture process would not occur, leading to carbon black largely retaining its agglomerated form. After 60 min of mixing, a large portion of the initially large carbon black agglomerates were broken down into small aggregates and primary particles (Fig. 3d and f). At high carbon loading, this also resulted in a higher surface coverage of NMC by C65 compared to lower loading (Fig. 3f).

Although it is apparent from SEM micrographs that dry mixing leads to carbon black deagglomeration to different extents, it is challenging to quantify the degree of deagglomeration. The difficulty lies in the imaging of particles of two different length scales i.e., micron-sized NMC particles and nano-sized carbon black particles. TEM is often deployed to image and study the structure of carbon black. However, as only a small observation region down to the nm-scale is possible, it is less practical in terms of an overall representative evaluation of the whole sample. Therefore, the selection of a proxy metric to evaluate and indirectly quantify carbon black deagglomeration could have great utility.

### 3.2. NMC622 bulk resistivity

The intrinsic resistivity of NMC is temperature-dependent and gradually increases with increasing temperature [1]. The bulk resistivity also differs from the intrinsic resistivity (i.e., individual particle resistivity) as the contact interfaces between particles contribute additional resistances to charge transport. For NMC622, the bulk electronic conductivity was reported to be between  $10^{-3}$  –  $10^{-2}$  S cm $^{-1}$ , corresponding to a resistivity of  $100{-}1000~\Omega$  cm, based on dense sintered pellets [1]. In this study, we found the resistivity of NMC622 powder compressed to a density of  $4.0~{\rm g~cm}^{-3}$  to be around  $528~\Omega$  cm. Although this value is in rough agreement with the values reported in the literature, it does not represent the actual intrinsic electronic conductivity, as complete contact between particles can never be achieved, even with high compression force.

Furthermore, the electronic conductivity of NMC is also state of lithiation dependent [44]. In general, resistivity decreases with increasing state of lithiation of NMC. This is attributed to the increase in Ni<sup>4+</sup> ions, leading to holes in the (Ni<sup>4+</sup>/Ni<sup>3+</sup>) band, and the decreased distance of Ni<sup>4+</sup>–O<sup>2-</sup> from higher covalency, making Ni<sup>3+</sup>–O<sup>2-</sup>–Ni<sup>4+</sup> hopping easier [45]. For NMC532 (relative sample density 96–98 %) with a reported electronic conductivity ( $\sigma$ ) of 1.3 x 10<sup>-3</sup> S cm<sup>-1</sup>, this corresponds to a state of lithiation of approximately 30–50 % (log  $\sigma$  = –2.89) [44]. Ni is considered an active conduction site that may help with electron hopping so NMC622 should possess a slightly higher conductivity than NMC532 at the same state of lithiation. Note that for NMC532, 622 and 811, their variation in electronic conductivity is minimal.

In this study, NMC622 has a log  $\sigma$  value of -2.72 based on the calculated resistivity at a sample density of 4.0 g cm $^{-3}$ . The relative density is approximately 85 % based on the true density of NMC622, and this resistivity showed minimal deviation with increasing compression, which was assumed to be representative of the bulk of the sample. This indicates that, here, the state of lithiation of NMC was estimated to also be between 30 and 50 %, potentially slightly lower than that of NMC532 in the referenced study [44]. However, the distribution of electronic conductivity is inhomogeneous within a single particle and, therefore, represents a variation in the state of lithiation on different parts of a single particle [46]. Despite this limitation, the estimated value still provides a useful rough indication of the average state of lithiation for the NMC particles used in this study.

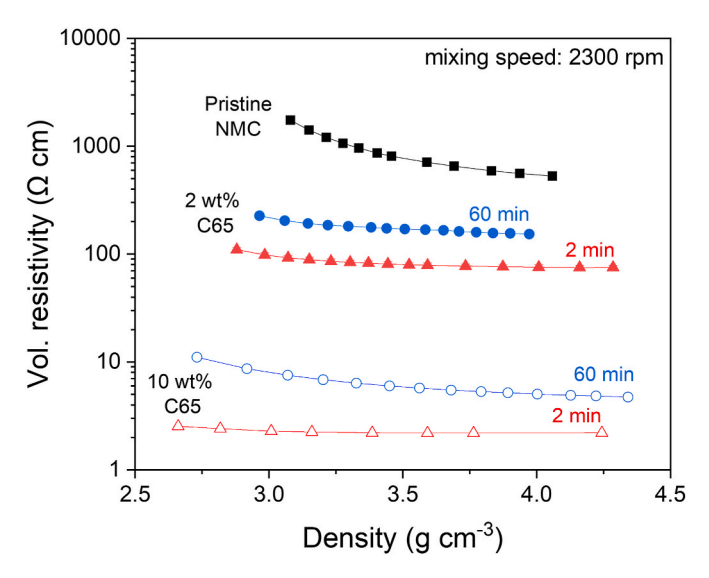


Fig. 4. Resistivity of pristine NMC and powder mixtures of NMC with 2 wt% and 10 wt% C65 both mixed for 2 and 60 min.

## 3.3. Effect of carbon loading

Fig. 4 shows the resistivity of pristine NMC622 along with binary mixtures of NMC622 containing 2 wt% and 10 wt% C65 (herein referred to as low and high carbon loading respectively). Samples were subjected to 2 and 60 min of mixing (herein referred to as short and long mixing respectively) at 2300 rpm. The two mixing times were selected as they represent the extremes within the broad mixing time studied and were shown to have significant differences in resistivity, which will be discussed in Section 3.5. In general, the addition of carbon black resulted in a significant decrease in the powder resistivity. Pristine NMC showed the highest resistivity, and resistivity decreased significantly by several orders of magnitude as the carbon loading increased from 2 wt% to 10 wt % C65. Carbon black has a lower resistivity compared to NMC particles and, therefore, forms a more efficient electronic pathway. Electrons experience less resistance and can travel more efficiently, leading to a decrease in the bulk powder resistivity. The density of the bulk powder increases with compression force due to improved packing of NMC622 and C65, which is attributed to particle rearrangement and partial fragmentation of agglomerates. At the same time, this results in an increase in the electrical interparticle contact, maximising the contact area between particles and potentially reducing the length of the pathways required for electron transfer or even establishing new electronic pathways.

For both low and high carbon loading samples, the resistivity for samples mixed for 2 min is lower than that of 60 min. The volume resistivity axis in Fig. 4 is presented in a logarithmic scale, which reflects that the difference for 2 wt% C65 is much larger than that for 10 wt% C65. This indicates that a short mixing time, corresponding to a low degree of deagglomeration, is favourable to achieving low resistivity. Fig. 4 also shows that there is a minimum resistivity, typically obtained beyond a density of 4.0 g cm<sup>-3</sup>, where the resistivity remains almost constant with increasing powder density. It is likely that at this density, a very high particle packing has been achieved, and therefore, the resistivity is representative of the entire sample volume. For low particle packing at low sample densities, there is a possibility of selective representation of resistivity. This observation is attributed to the resistivity of the NMC622, and therefore, the resistivity of the binary powder mixture will not approach the conductivity of pure C65. When approaching very high carbon black loadings, the bulk resistivity is likely to be dominated by the resistivity of carbon black. However, electrons are still likely to come into contact and travel through NMC622 particles, which will increase the resistance experienced by

electrons. This value represents the lowest resistivity that can be achieved for a specific carbon loading, mixing technique and process conditions. With increasing carbon black loading, the electronic pathways for electron transfer will increasingly be made up of long "chain-like" structures of carbon black agglomerates and are less likely to travel through NMC622 particles. Nevertheless, the minimum resistivity is almost constant, which can also be observed in a typical percolation curve as shown in Fig. 1. Upon reaching the percolation threshold, the change in resistivity becomes less apparent and eventually remains constant when approaching very high conductive additive content.

### 3.4. Effect of sample loading

Carbon black deagglomeration ultimately depends on the overall energy input of the mixing process. To study the effect of sample loading on deagglomeration, the conductive additive content (2 wt% C65) and mixing speed (2300 rpm) were kept constant while the total sample mass loading was varied. Fig. 5 shows a similar trend as described previously in Section 3.3, where 2 min mixing yielded a lower resistivity, and 60 min yielded a higher resistivity. The results also suggest that an increase in powder sample loading led to a slight increase in resistivity. For example, for 60 min mixing, a sample loading of 20 g showed the lowest resistivity, followed by an increase for 50 g and 100 g. This difference is less distinct for samples mixed for 2 min, as the degree of deagglomeration of carbon black between the different sample loadings is not as significant within a short time.

Increasing the sample loading with the same formulation corresponds to an increase in the overall number of carbon black agglomerates. The total energy input into the system is constant with identical process conditions, resulting in a lower specific energy supplied to the agglomerates as the amount of carbon black increases. Increasing the total loading leads to a lack of free space available for particles to move and interact. As a result, the change in the mixing profile can lead to less shear forces generated and less uniform mixing. These can lead to a less efficient deagglomeration process, affecting the subsequent dispersion and coating onto NMC622.

Conversely, underloading can impact the shear rate, especially in a system where large NMC particles and small C65 particles are present. A higher specific energy input may be experienced by the particles, resulting in more intense interactions that may cause particle breakage. It is also possible that the energy input is wasted due to insufficient interactions between particles. It is a balance between maximising

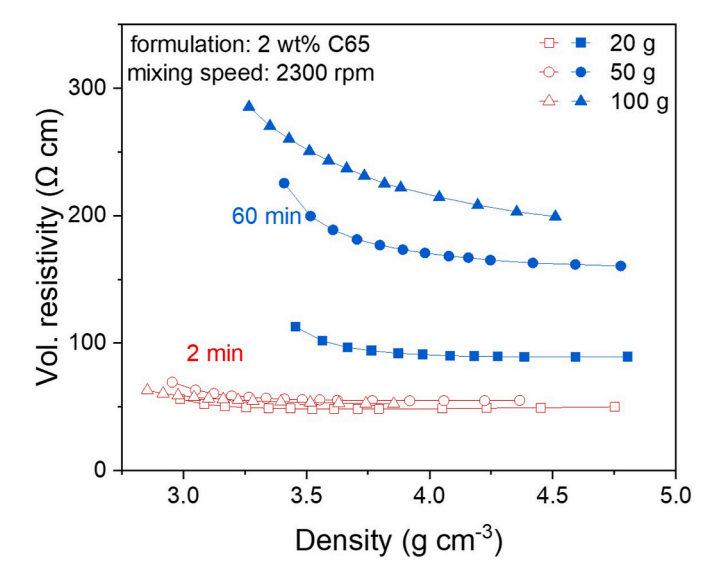


**Fig. 5.** Resistivity of powder mixtures with varying sample loading and mixing times of 2 and 60 min.

process output and achieving consistent, optimal shear rates to enhance mixing performance. Therefore, it is important to develop a mechanistic understanding of how mechanofusion process parameters, combined with sample formulation and loading, affect mixing efficiency.

### 3.5. Effect of mechanofusion process parameters

Mixing process parameters play a significant role in determining the number and probability of interactions that occur between particles. The total energy input into the binary powder mixture is controlled by the mixing time and mixing speed. Prolonged mixing time maximises the amount of energy input while increased mixing speed leads to higher shear rates for more intense mixing.

Fig. 6a shows a binary mixture of NMC622 with 2 wt% C65, without the aid of mechanofusion mixing (0 min), with the highest resistivity of 171.1  $\Omega$  cm at a density of 4.0 g cm $^{-3}$ . For samples subjected to mechanofusion mixing at 2300 rpm, an increase in resistivity with mixing time was observed. In the cases studied, samples mixed for the shortest time of 2 min showed the lowest resistivity of 75.7  $\Omega$  cm, while samples subjected to long mixing times of 30 and 60 min showed the highest, and similar resistivities of 156.4 and 153.4  $\Omega$  cm respectively. A similar result was obtained for samples mixed at high carbon loading, where 2 min mixing showed the lowest resistivity across all mixing times, as shown in Fig. 6b. From these findings, it is concluded that a short mixing time is favourable to achieving low resistivity for micronsized NMC622 with nano-sized carbon black.

An implication of these findings is that uniform dispersion is not necessary, as supported by Huang et al. for the case of conductive applications [25]. Dannenberg [47] proposed that there is an optimum dispersion time before agglomerates are broken down and the distance between particles is increased. Cembrola [48] stated that the dispersion process must be carefully controlled to avoid under or over-dispersion of carbon black which may affect conductivity. Uniform dispersion is usually achieved by a prolonged time of mixing, which may include higher energy input to achieve a high degree of deagglomeration, resulting in a homogenous mixture and narrow particle size distribution. Short mixing yielding low resistivity implies that only minimal agglomeration is required, and most of the carbon black within the mixture should remain in larger structures. This also implies that there is an optimum combination of small and large carbon black structures that constitutes the optimal combination of electronic pathways.

The resistivities for both carbon loading samples, at various mixing times, at a sample density of 4.0 g cm $^{-3}$ , were extracted and are presented in Fig. 6c and d. For low carbon loading, the resistivity is more sensitive to mixing time compared to high carbon loading. This is evident in Fig. 6c with a large increase in resistivity of 75.7  $\Omega$  cm to 153.4  $\Omega$  cm, when mixing time is increased from 2 min to 60 min respectively. The increase in resistivity with mixing time can be firstly explained by a higher degree of deagglomeration of carbon black. Carbon black exists as long, "chain-like" structures within the interparticle voids of NMC particles. These structures act as an interconnected electronic network that facilitates electron movement. When deagglomeration of these structures occurs, this interconnected network is said to be disrupted, thus resulting in a disconnected electronic pathway. Prolonged mixing can also increase the spheronisation effect of mechanofusion, resulting in a smoother active particle surface. Initially, carbon

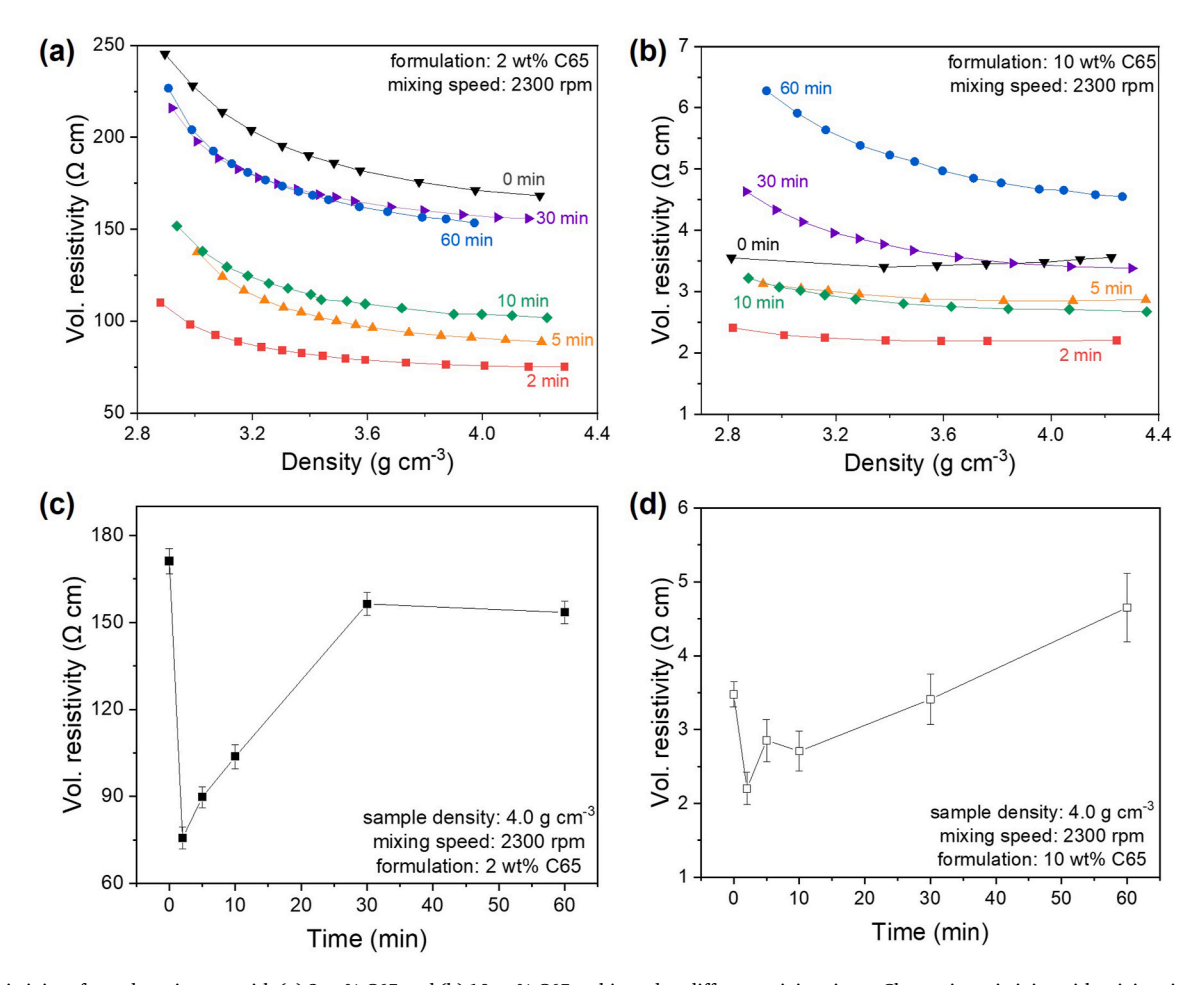


Fig. 6. Resistivity of powder mixtures with (a) 2 wt% C65 and (b) 10 wt% C65, subjected to different mixing times. Change in resistivity with mixing time for powder mixtures of NMC with (c) 2 wt% and (d) 10 wt% C65.

black rupture takes place, and large agglomerates are broken down into smaller constituents. They also start to attach to the surface of NMC due to high compression forces as the particles are forced through the converging space. Prolonged mixing then results in erosion, gradually reducing these aggregates into smaller particles and continued compression leads to compaction of the carbon black coating. The carbon-coated NMC surface is consistently sheared and polished during the mixing process, which results in a reduction in surface area. In comparison with loosely bound carbon black "chain-like" structures on the particle surface, the smooth carbon-coated surface limits contact area with other surrounding particles. In addition to the smaller carbon structures resulting from mechanofusion mixing, the effect of increased resistivity is more apparent.

For high carbon loading, the resistivity increases from 2.2  $\Omega$  cm to 4.6  $\Omega$  cm at 2 min and 60 min respectively, as shown in Fig. 6d. The bulk resistivity is dominated by carbon black at high carbon loading. An increase in carbon black agglomerates with the same energy input results in slower deagglomeration of these agglomerates. Thus, a higher proportion of large carbon black structures are retained, forming the interconnected electron pathway. Since carbon black has a relatively higher electronic conductivity compared to NMC particles, the resistance to electron movement is lower. The higher the probability of electrons travelling through NMC particles, the higher the resistance experienced compared to a pathway constituted mainly of conductive additive.

The relationship between mixing speed and resistivity is dependent on the carbon black loading. Grießl et al. [28] demonstrated the interdependency between carbon black loading and the blade circumferential speed. For 2 wt% C65, mixing time is a key consideration when selecting the optimal mixing speed as shown in Fig. 7a. For comparison purposes, mixing speeds of 1000, 2300 and 5000 rpm are categorised as low, medium, and high speeds respectively.

For short mixing times, medium to high speeds are desired, while lower speeds are desired for long mixing times. The selection of mixing speeds and times can be related to achieving a similar energy input required for adequate mixing to achieve low resistivity. If low mixing speeds are required for long mixing times, this implies that similar energy input is needed for high mixing speeds to achieve a similar degree of deagglomeration and the corresponding resistivity. Therefore, it can be deduced that high mixing speeds, where the shear rate and energy input are much higher, should require a short mixing time to achieve a similar mixing intensity.

A different observation applies to high carbon loading samples. The lowest resistivity was obtained at low mixing speeds, regardless of the mixing time, as shown in Fig. 7b. The resistivity remains constant with increasing speeds at short mixing times but increases sharply at long mixing times. The percolated electronic pathways are formed mainly by carbon black, and low mixing speeds result in very little deagglomeration compared to low carbon loading. As a result, there is a higher probability of large carbon black structures remaining after mixing and retaining the interconnected electronic pathways (Fig. 7c). At a mixing speed of 1000 rpm, a large portion of carbon black agglomerates is still present after 2 min mixing, which may be attributed to insufficient shear stress for rupture (Fig. S1). After 60 min mixing, aggregates were observed, indicating that prolonged mixing led to sufficient energy for deagglomeration (Fig. S1). This is evident from Fig. 7b where similar resistivities were obtained for both 2 and 60 min samples mixed at 1000 rpm. However, as powders are subjected to resistivity by compression measurements, these long-chain structures can still be re-established to form the interconnected network.

Increasing the mixing speed corresponds to an increase in shear rates [49]. Prolonged mixing results in a relatively higher degree of deagglomeration, resulting in agglomerates giving large aggregates. This represents a disruption to these interconnected pathways, where the long-chain structures are no longer present. In this case, even though the percolated pathways still exist, electrons have an increased probability of travelling through NMC particles, leading to increased resistivity (Fig. 7d). SEM micrographs show that a large amount of carbon black was deagglomerated and coated onto NMC, which is evident from large particles with smooth surfaces due to C65 filling the surface pores of NMC, followed by the spheronisation effect of mechanofusion mixing at 60 min and 5000 rpm (Fig. S2). Although the resistivity of these particles

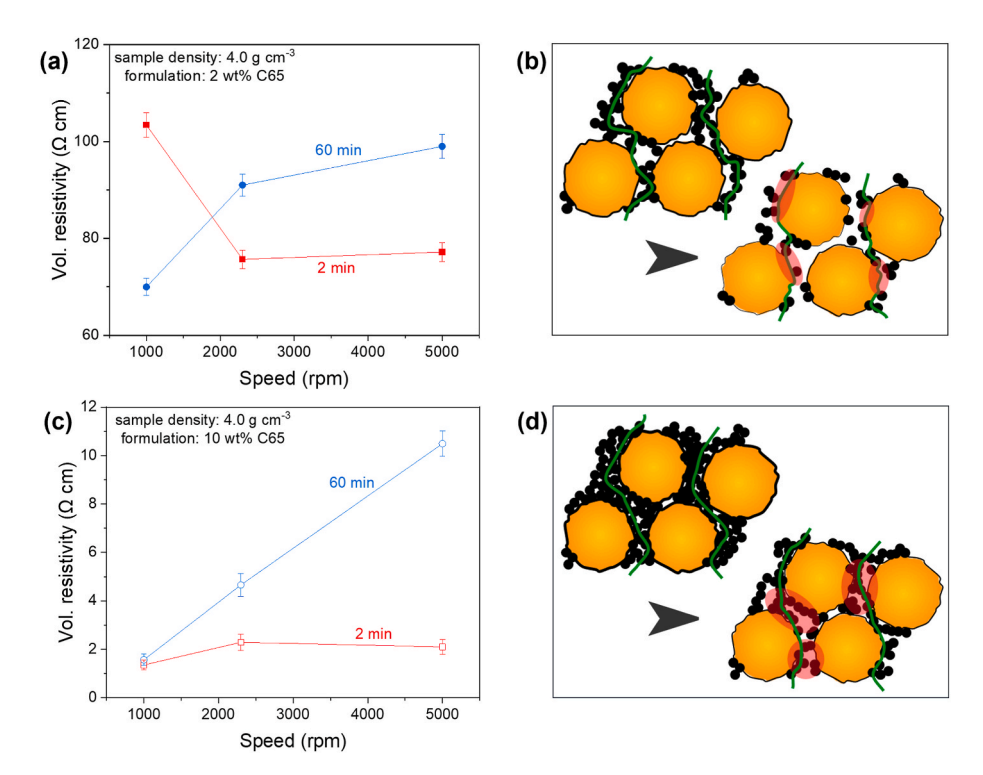


Fig. 7. Change in resistivity with mixing speed for powder mixtures of (a) 2 wt% and (b) 10 wt% C65. Schematics depict the change in interconnected pathways formed by carbon black after mixing for (c) low and (d) high carbon loading.

is very low, it likely has a detrimental effect on ionic conductivity due to the inaccessibility of NMC, limiting the surface area in contact with electrolyte when fabricated into electrodes.

The shear rate and energy input are dictated by the mixing speed. High shear mixing speeds are often linked to the power input and tip speed of the rotor [50]. The dimensionless Froude-tool number has been used as a method of quantifying mixing intensity between different techniques. It is defined as the ratio of inertia forces to gravitational forces, and for mechanofusion can be defined as [51,52]:

$$\operatorname{Fr}_{t} = \frac{\omega_{t}^{2} r_{t}}{\sigma} \tag{3}$$

where  $\omega_t$  is the rotor speed,  $r_t$  is the rotor radius and g is the gravitational constant.

In this study, the rotor radius ( $r_t$ ) was kept constant, and therefore, the higher the Fr $_t$  indicates the higher the mixing intensity is. Westphal et al. [18] found that dry mixing graphite with carbon black has minimal effect on electrode resistivity up to Fr $_t$  due to only homogenisation of powders but resistivity increases at higher Fr $_t$ . Haselrieder et al. [51] found that structural changes of carbon black agglomerates and coating onto NMC surfaces can be observed in cathodes consisting of particles processed with a low Fr $_t$  of 50 for 2 and 8 min mechanofusion mixing. The findings also complement the observations reported by Bockholt et al. with a Fr $_t$  of 400 [53]. Powder packing density was increased, but the conductance of powders remained low.

While the use of Frt has been studied on electrode resistivity and the

interactions between graphite-carbon black and NMC-carbon black are vastly different, a similar approach can be taken to establish the relationship between  $Fr_t$  and powder resistivity of a binary powder mixture of active material and conductive additive. In this study, a  $Fr_t$  of around 50 (speed: 1000 rpm) represents the region where the lowest resistivity can be achieved for all cases, except at low carbon loading with short mixing times. For this specific case, an  $Fr_t$  of 260 (speed: 2300 rpm) up to around 1230 (speed: 5000 rpm) is more favourable for achieving low resistivity. The  $Fr_t$  is less important as mixing does not greatly affect the resistivity and, thus, the carbon black structures for this condition.

For  ${\rm Fr_t} > 6$ –7, corresponding to a mixing speed of approximately 350 rpm, powders are already centrifugated and form an annulus on the mixer wall. The  ${\rm Fr_t}$  ranges of 260–1230 show that the centrifugal force is several magnitudes higher than the gravity force during mechanofusion mixing. At these ranges, the high shear mixing is very intense, which results in deagglomeration. In general, a high  ${\rm Fr_t}$  is preferred for short mixing, and a low  ${\rm Fr_t}$  is preferred for long mixing, regardless of carbon loading. The results complement the literature discussed, beyond a certain  ${\rm Fr_t}$ , the resulting resistivity is similar. Therefore, it can be inferred that the structure of carbon black is also similar and thus indicates a similar degree of carbon black deagglomeration.

#### 3.6. Electrochemical performance

The effect of mechanofusion process conditions on the electrochemical performance of electrodes containing carbon-coated NMC particles was evaluated. Electrodes were fabricated with a formulation

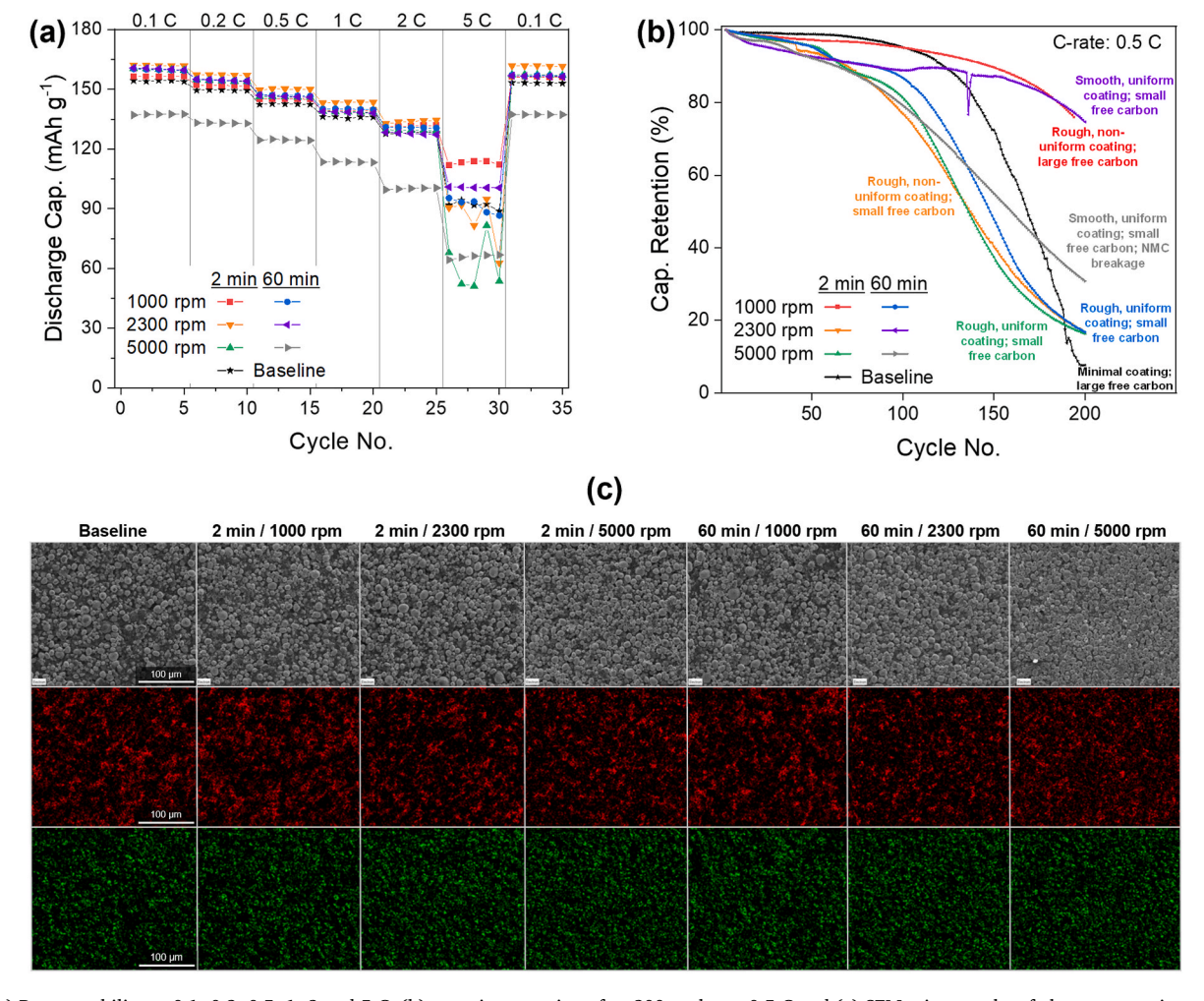


Fig. 8. (a) Rate capability at 0.1, 0.2, 0.5, 1, 2 and 5 C, (b) capacity retention after 200 cycles at 0.5 C and (c) SEM micrographs of element mapping areas (top), carbon mapping (middle) and oxygen mapping (bottom) of electrodes with different mixing formulations.

of 96:2:2 wt% NMC:C65:PVDF using carbon-coated NMC through wet slurry mixing. This corresponds to a theoretical formulation of 94.1:3.9:2 wt% NMC:C65:PVDF. Standard baseline electrodes with the identical theoretical formulation were also prepared for comparison.

Fig. 8a shows the rate capabilities of the electrodes with formulations of different carbon-coated NMC particles. In general, except for the extreme dry mixing condition of 5000 rpm/60 min, all electrodes exhibited a similar capacity at lower C-rates (below 2 C) and were higher than the baseline electrode. This trend suggests that the carbon coating on the NMC surface improves electrochemical performance through better electronic conduction.

At a higher C-rate of 5 C, electrodes with NMC processed at 1000 rpm/2 min and 2300 rpm/60 min exhibited significantly better performance than all other formulations, including the baseline electrode. Specifically, the electrode containing formulation of 1000 rpm/2 min, despite having a higher powder resistivity, showed the best rate capability at 5 C. This is likely due to the rough, incomplete coverage of carbon coating, which enhances electronic conductivity, but also provides sufficient NMC surface area for contact with electrolyte for good ionic conduction. Similarly, the electrode with 2300 rpm/60 min formulation, which had higher powder resistivity, also demonstrated improved rate capability at 5 C due to the increased amount of carbon coating, which potentially enhanced short-range conduction at high Crates. These observations highlight the importance of the presence of short-range electronic pathways, which enhance electrochemical performance. This also demonstrates the influence of the extent of carbon coating and the free carbon structures present, on the electrochemical performance of the electrodes.

The long-term cycling performance of the electrodes was evaluated over 200 cycles at 0.5 C as shown in Fig. 8b. The electrodes with formulations of 1000 rpm/2 min and 2300 rpm/60 min showed superior capacity retention of 78.6 and 77.9 % respectively after 190 cycles. These electrodes also exhibited stable capacity retention after an initial decrease, suggesting that the carbon coating improves long-term cycling stability of the electrodes. This is in contrast with the baseline electrode, where an initial high retention up to 100 cycles was observed, but starts to degrade rapidly beyond that.

All electrodes with other formulations degraded rapidly after 50 cycles, which is inferior compared to the baseline electrode in terms of capacity retention. Particularly, the electrode with the most intense mixing formulation (5000 rpm/60 min), exhibited a different degradation profile with continuous degradation and no stable retention throughout the cycle life. This could be attributed to the partial breakage of NMC particles in the dry mixing process and the resulting smooth NMC surface from spheronisation (Fig. S2), limiting ionic conductivity and leading to high overpotentials and thus active material degradation at high C-rates. Nevertheless, all electrodes with carbon-coated NMC still exhibited better capacity retention compared to the baseline electrode after 200 cycles.

The observed improvements in both rate capability and capacity retention are likely due to the reduction in overpotentials facilitated by the carbon coating from mechanofusion. The conductive coating enhances electron transport across the NMC surface, promoting shortrange electrical contacts with the surrounding CBD and improving connections between NMC particles throughout the electrode. This reduction in electronic resistance leads to lower ohmic losses, particularly under the high current studied (5 C). The conductive carbon coating could also potentially enhance charge transfer reactions which lead to a reduction in the charge transfer overpotentials. Additionally, the carbon coating also potentially reduces any side reactions with the electrolyte, thus stabilising the particle interfaces and mitigating any overpotential buildup. In short, the carbon coating can help reduce the local overpotentials on the relatively large NMC particles which are prone to polarisation and uneven current distribution where an uneven distribution of conductive networks is present. These can all help to preserve the structural and electrochemical integrity of the NMC over

long-term cycling, thus enhancing both high-rate performance and cycling stability of the electrode.

While most electrodes with carbon-coated NMC benefit from the conductive coating in terms of electronic conductivity and performance, the two formulations processed at 1000 rpm/2 min and 2300 rpm/60 min were the most effective based on the electrochemical performance. Fig. 8c shows the SEM-EDX elemental mapping of the electrodes, indicating that the strongest carbon signal originates from large, fluffy CBD bridge structures between NMC particles, while particle surfaces exhibit weak C signals. This may indicate thin or non-uniform coatings below the mapping detection sensitivity. For 1000 rpm/2 min, SEM-EDX and powder resistivity trends suggest a low amount of coating combined with a large amount of free carbon, which forms extensive bridge structures for long-range conduction while maintaining electrolyte access to NMC surface. For 2300 rpm/60 min, a higher degree of coating, along with smaller free carbon structures that form smaller bridge structures within the NMC voids to enhance long-range conduction. Supplementary SEM micrographs of carbon-coated NMC particles processed at different conditions can be found in Fig. S3.

In other formulations, carbon coatings and bridge structures are still present, but their proportions and spatial distribution are likely suboptimal for achieving a favourable balance of electronic pathways. For instance, when large bridge structures dominate and particle coating is minimal, short-range electronic conduction at the particle interface may be limited, leading to high interfacial resistance. In contrast, excessive coating with insufficient bridge structures may favour short-range conduction but hinder ionic transport. This suboptimal balance between short and long-range pathways likely accounts for the inferior rate capability and cycling stability. The results suggest that the two optimal formulations achieve a more effective balance, consistent with the proposed CBD architecture in Section 1, where both film-like coatings for short-range conduction and bridge-like structures for long-range conduction are essential for optimal performance.

It is worth noting, however, that the coating can also influence ionic transport to some extent, particularly if it is highly dense, potentially impeding ionic conduction and contributing to poor cell performance. Thus, an ideal film structure coating should either be a thin, uniformly distributed coating or a non-uniform coating with incomplete coverage. This is supported by the electrode with 2300 rpm/60 min formulation, where a smooth and uniform coating is complemented by small free carbon structures that form extensive bridge structures within smaller voids between NMC. Similarly, the electrode with 1000 rpm/2 min formulation showed excellent performance, likely due to a rough, moderately distributed coating that is sufficient to enhance short-range electronic conduction while still facilitating effective ionic transport. The resulting free carbon structures are larger and can therefore contribute to more bridge structures for long-range conduction. Further investigation is required to systematically examine how coating properties, such as thickness, porosity and uniformity, affect ionic conductivity of the carbon-coated NMC electrodes.

### 4. Conclusions

Deagglomeration of carbon black involves a complex interplay of process parameters and material properties, such as carbon black loading, mixing time and speed, with appropriate characterisation methods. To the best of our knowledge, this is the first mechanistic study on the use of mechanofusion for carbon black deagglomeration as a means of tailoring film structures for short-range electrical contacts. From the findings of this study, the following conclusions are drawn:

 The deagglomeration behaviour for nano-sized carbon black C65 with micron-sized NMC622 is strongly dependent on the overall energy input, largely dictated by mixing time and speed. The degree of carbon black dispersion plays a crucial role in determining the formation of conductive networks within the electrode structure.

- The optimal mixing speed and time to minimise powder resistivity depend strongly on carbon loading: high speeds with short mixing times are most effective for low carbon loading, whereas low speeds with long mixing times are more suitable for high carbon loading.
- 3. For high-power and energy density electrodes, minimal carbon black (<2 wt%) is desirable to maximise active material content. While powder resistivity correlates with deagglomeration, it does not directly predict electrochemical performance, particularly for wet electrodes, which is instead governed by the balance of short and long-range electronic pathways.
- 4. Electrodes with a well-balanced distribution of short and long-range conductive pathways, i.e., formulations of 1000 rpm/2 min and 2300 rpm/60 min, demonstrated improved rate capability and capacity retention despite higher powder resistivity, likely due to reduced local overpotentials.
- The findings apply only to micron-sized active material and nanosized conductive additives. The interactions between both nanosized active material and conductive additives remain an interesting avenue to be explored.

This study presents a different approach to characterising carbon black deagglomeration, departing from conventional metrics like slurry properties. A more comprehensive understanding of the technical aspects associated with carbon black dispersion, as concluded above, serves as guidance to improve the efficiency of the battery manufacturing process. While powder resistivity correlates with carbon black deagglomeration, it does not directly predict electrochemical performance. Optimal electrochemical results depend on balancing short and long-range conductive pathways. This work offers insights into the link between carbon black dispersion, powder properties, and cell performance for future research on active material and conductive additive interactions, conductive network design, and dry electrode manufacturing for next-generation lithium-ion batteries.

### CRediT authorship contribution statement

**Guo J. Lian:** Writing – review & editing, Writing – original draft, Visualization, Validation, Project administration, Methodology, Investigation, Formal analysis. **Prateek Verma:** Validation, Investigation, Formal analysis. **Denis Cumming:** Writing – review & editing, Supervision, Resources, Funding acquisition, Conceptualization. **Rachel M. Smith:** Writing – review & editing, Supervision, Resources, Funding acquisition, Conceptualization.

### Declaration of competing interest

The authors declare the following financial interests/personal relationships which may be considered as potential competing interests. Rachel M. Smith reports financial support was provided by The Faraday Institution. Denis Cumming reports financial support was provided by The Faraday Institution. Prateek Verma reports financial support was provided by The Faraday Institution. If there are other authors, they declare that they have no known competing financial interests or personal relationships that could have appeared to influence the work reported in this paper.

### Acknowledgements

The authors would like to thank the Faraday Institution for the financial support provided towards the "Nextrode" project (Grant number: FIRG015) and the Faraday Undergraduate Summer Experience project (Grant number: FITG-FUSE138). The authors would also like to acknowledge Dr Xuesong Lu, Dr Milan K. Sadan and Dr Kate Pitt for valuable discussions, Charlie Stothard for providing technical support, and the Sorby Centre for Electron Microscopy at the University of Sheffield for their facilities.

#### Appendix A. Supplementary data

Supplementary data to this article can be found online at https://doi.org/10.1016/j.jpowsour.2025.238311.

### Data availability

Data will be made available on request.

#### References

- S. Wang, M. Yan, Y. Li, C. Vinado, J. Yang, Separating electronic and ionic conductivity in mix-conducting layered lithium transition-metal oxides, J. Power Sources 393 (Jul. 2018) 75–82, https://doi.org/10.1016/j.jpowsour.2018.05.005.
- [2] J. Asenbauer, T. Eisenmann, M. Kuenzel, A. Kazzazi, Z. Chen, D. Bresser, The success story of graphite as a lithium-ion anode material-fundamentals, remaining challenges, and recent developments including silicon (oxide) composites, Sustain. Energy Fuels 4 (11) (2020) 5387–5416, https://doi.org/10.1039/dose00175a.
- [3] S. Yari, et al., Constructive versus destructive heterogeneity in porous electrodes of lithium-ion batteries, ACS Appl. Energy Mater. 3 (12) (2020) 11820–11829, https://doi.org/10.1021/acsaem.0c01966.
- [4] S. Müller, J. Eller, M. Ebner, C. Burns, J. Dahn, V. Wood, Quantifying inhomogeneity of lithium ion battery electrodes and its influence on electrochemical performance, J. Electrochem. Soc. 165 (2) (Jan. 2018) A339, https://doi.org/10.1149/2.0311802ies.
- [5] M. Duquesnoy, I. Boyano, L. Ganborena, P. Cereijo, E. Ayerbe, A.A. Franco, Machine learning-based assessment of the impact of the manufacturing process on battery electrode heterogeneity, Energy AI 5 (Sep. 2021) 100090, https://doi.org/ 10.1016/j.egyai.2021.100090.
- [6] W. Bauer, D. Nötzel, V. Wenzel, H. Nirschl, Influence of dry mixing and distribution of conductive additives in cathodes for lithium ion batteries, J. Power Sources 288 (Aug. 2015) 359–367, https://doi.org/10.1016/j.jpowsour.2015.04.081.
- [7] R.M. Saraka, S.L. Morelly, M.H. Tang, N.J. Alvarez, Correlating processing conditions to Short- and long-range order in coating and drying lithium-ion batteries, ACS Appl. Energy Mater. 3 (12) (Dec. 2020) 11681–11689, https://doi. org/10.1021/acsaem.0c01305.
- [8] J. Entwistle, R. Ge, K. Pardikar, R. Smith, D. Cumming, Carbon binder domain networks and electrical conductivity in lithium-ion battery electrodes: a critical review, Renew. Sustain. Energy Rev. 166 (Sep) (2022), https://doi.org/10.1016/j. rser\_2022.112624.
- [9] J. F. Baumgärtner, K. V. Kravchyk, and M. V. Kovalenko, 'Navigating the carbon maze: a roadmap to effective carbon conductive networks for lithium-ion batteries', Adv. Energy Mater., vol. n/a, no. n/a, p. 2400499, doi: 10.1002/ aenm.202400499.
- [10] S.L. Morelly, N.J. Alvarez, M.H. Tang, Short-range contacts govern the performance of industry-relevant battery cathodes, J. Power Sources 387 (January) (2018) 49–56, https://doi.org/10.1016/j.jpowsour.2018.03.039.
- [11] X. Lu, et al., Effect of carbon blacks on electrical conduction and conductive binder domain of next-generation lithium-ion batteries, J. Power Sources 592 (Feb. 2024) 233916, https://doi.org/10.1016/j.jpowsour.2023.233916.
- [12] X. Lu, et al., Microstructure of conductive binder domain for electrical conduction in next-generation lithium-ion batteries, Energ. Tech. (Aug. 2023) 2300446, https://doi.org/10.1002/ente.202300446.
- [13] R. Ge, et al., Numerical design of microporous carbon binder domains phase in composite cathodes for lithium-ion batteries, ACS Appl. Mater. Interfaces 15 (23) (Jun. 2023) 27809–27820, https://doi.org/10.1021/acsami.3c00998.
- [14] R. Ge, A.M. Boyce, Y. Shui Zhang, P.R. Shearing, D.J. Cumming, R.M. Smith, Discrete element method and electrochemical modelling of lithium ion cathode structures characterised by X-ray computed tomography, Chem. Eng. J. 465 (Jun. 2023) 142749, https://doi.org/10.1016/j.cej.2023.142749.
- [15] H.-S. Kim, K. Kim, S.-I. Moon, I.-J. Kim, H.-B. Gu, A study on carbon-coated LiNi1/ 3Mn1/3Co1/3O2 cathode material for lithium secondary batteries, J. Solid State Electrochem. 12 (7) (Aug. 2008) 867–872, https://doi.org/10.1007/s10008-008-0552-0.
- [16] S.A. Hong, D.H. Kim, K.Y. Chung, W. Chang, J. Yoo, J. Kim, Toward uniform and ultrathin carbon layer coating on lithium iron phosphate using liquid carbon dioxide for enhanced electrochemical performance, J. Power Sources 262 (2014) 219–223, https://doi.org/10.1016/j.jpowsour.2014.03.132.
- [17] S.-M. Oh, S.-W. Oh, C.-S. Yoon, B. Scrosati, K. Amine, Y.-K. Sun, High-Performance Carbon-LiMnPO4 nanocomposite cathode for lithium batteries, Adv. Funct. Mater. 20 (19) (2010) 3260–3265, https://doi.org/10.1002/adfm.201000469.
- [18] B.G. Westphal, et al., Influence of high intensive dry mixing and calendering on relative electrode resistivity determined via an advanced two point approach, J. Energy Storage 11 (Jun. 2017) 76–85, https://doi.org/10.1016/j. est.2017.02.001.
- [19] M. Ali, L. Lin, D. Cartridge, High electrical conductivity waterborne dispersions of carbon black pigment, Prog. Org. Coating 129 (Apr. 2019) 199–208, https://doi. org/10.1016/j.porgcoat.2018.12.010.
- [20] A. Awarke, S. Lauer, S. Pischinger, M. Wittler, Percolation–tunneling modeling for the study of the electric conductivity in LiFePO4 based Li-ion battery cathodes, J. Power Sources 196 (1) (Jan. 2011) 405–411, https://doi.org/10.1016/j. jpowsour.2010.07.048.

- [21] A. Alekseev, T.H. Wu, L.G.J. van der Ven, R.A.T.M. van Benthem, G. de With, Global and local conductivity in percolating crosslinked carbon black/ epoxy-amine composites, J. Mater. Sci. 55 (21) (Jul. 2020) 8930–8939, https:// doi.org/10.1007/s10853-020-04650-2.
- [22] H.-J. Choi, M.S. Kim, D. Ahn, S.Y. Yeo, S. Lee, Electrical percolation threshold of carbon black in a polymer matrix and its application to antistatic fibre, Sci. Rep. 9 (1) (Apr. 2019) 6338, https://doi.org/10.1038/s41598-019-42495-1.
- [23] M. Haghgoo, R. Ansari, M.K. Hassanzadeh-Aghdam, Predicting effective electrical resistivity and conductivity of carbon nanotube/carbon black-filled polymer matrix hybrid nanocomposites, J. Phys. Chem. Solid. 161 (Feb. 2022) 110444, https://doi. org/10.1016/j.jpcs.2021.110444.
- [24] S. Akhtar, W. Lee, M. Kim, M.S. Park, W.S. Yoon, Conduction mechanism of charge carriers in electrodes and design factors for the improvement of charge conduction in li-ion batteries, J. Electrochem. Sci. Technol. 12 (1) (2021) 1–20, https://doi. org/10.33961/jecst.2020.01564.
- [25] M. Lowell, Carbon black filled conducting polymers and polymer blends 21 (4) (2002) 299–313, https://doi.org/10.1002/adv.10025.
- [26] A. Kasgoz, D. Akin, A. Durmus, Rheological and electrical properties of carbon black and carbon fiber filled cyclic olefin copolymer composites, Compos. B Eng. 62 (Jun. 2014) 113–120, https://doi.org/10.1016/j.compositesb.2014.02.017.
- [27] J.K. Mayer, et al., Influence of the carbon black dispersing process on the microstructure and performance of Li-Ion battery cathodes, Energy Technol. 8 (2) (2020) 1–11, https://doi.org/10.1002/ente.201900161.
- [28] D. Grießl, K. Huber, R. Scherbauer, A. Kwade, Dispersion kinetics of carbon black for the application in lithium-ion batteries, Adv. Powder Technol. 32 (7) (Jul. 2021) 2280–2288, https://doi.org/10.1016/j.apt.2021.05.003.
- [29] J.K. Mayer, H. Bockholt, A. Kwade, Inner carbon black porosity as characteristic parameter for the microstructure of lithium-ion electrodes and its effect on physical and electrochemical properties, J. Power Sources 529 (May 2022) 231259, https://doi.org/10.1016/j.jpowsour.2022.231259.
- [30] M. Weber, J.K. Mayer, A. Kwade, The carbon black dispersion index DICB: a novel approach describing the dispersion progress of carbon black containing battery slurries, Energy Technol. (2023), https://doi.org/10.1002/ente.202201299.
- [31] H. Bockholt, W. Haselrieder, A. Kwade, Intensive powder mixing for dry dispersing of carbon black and its relevance for lithium-ion battery cathodes, Powder Technol. 297 (2016) 266–274, https://doi.org/10.1016/j.powtec.2016.04.011.
- [32] M.E. Spahr, D. Goers, A. Leone, S. Stallone, E. Grivei, Development of carbon conductive additives for advanced lithium ion batteries, J. Power Sources 196 (7) (Apr. 2011) 3404–3413, https://doi.org/10.1016/j.jpowsour.2010.07.002.
- [33] C. Lischka, S. Gerl, J. Kappes, A. Chauhan, H. Nirschl, Experimental & simulative assessment of mixing quality for dry Li-Ion cathode production in an eirich intensive mixer, Powder Technol. 431 (Jan. 2024) 119072, https://doi.org/ 10.1016/j.powtec.2023.119072.
- [34] B. Marinho, M. Ghislandi, E. Tkalya, C.E. Koning, G. de With, Electrical conductivity of compacts of graphene, multi-wall carbon nanotubes, carbon black, and graphite powder, Powder Technol. 221 (May 2012) 351–358, https://doi.org/ 10.1016/j.powtec.2012.01.024.
- [35] S.P. Rwei, I. Manas-Zloczower, D.L. Feke, Observation of carbon black agglomerate dispersion in simple shear flows, Polym. Eng. Sci. 30 (12) (Jun. 1990) 701–706, https://doi.org/10.1002/pen.760301202.
- [36] J.J. Kuo, S.D. Kang, W.C. Chueh, Contact resistance of Carbon–Lix(Ni,Mn,Co)O2 interfaces, Adv. Energy Mater. 12 (31) (Aug. 2022), https://doi.org/10.1002/
- [37] S. Kane, S. Warnat, C. Ryan, Improvements in methods for measuring the volume conductivity of electrically conductive carbon powders, Adv. Powder Technol. 32 (3) (Mar. 2021) 702–709, https://doi.org/10.1016/j.apt.2021.01.016.

- [38] N. Mainusch, et al., New contact probe and method to measure electrical resistances in battery electrodes, Energy Technol. 4 (12) (2016) 1550–1557, https://doi.org/10.1002/ente.201600127.
- [39] C.D. Reynolds, S.D. Hare, P.R. Slater, M.J.H. Simmons, E. Kendrick, Rheology and structure of Lithium-ion battery electrode slurries, Energy Technol 10 (10) (2022) 2200545, https://doi.org/10.1002/ente.202200545.
- [40] T. Beuse, M. Fingerle, C. Wagner, M. Winter, M. Börner, Comprehensive insights into the porosity of lithium-ion battery electrodes: a comparative study on positive electrodes based on LiNi0.6Mn0.2Co0.2O2 (NMC622), Batteries 7 (4) (Dec. 2021), https://doi.org/10.3390/batteries7040070.
- [41] S. Lu, D.D.L. Chung, Viscoelastic behavior of carbon Black and its relationship with the aggregate size, Carbon 60 (Aug. 2013) 346–355, https://doi.org/10.1016/j. carbon.2013.04.047.
- [42] J. López-de-Uralde, et al., Automatic morphological categorisation of carbon Black nano-aggregates, in: P.G. Bringas, A. Hameurlain, G. Quirchmayr (Eds.), Database and Expert Systems Applications, Springer, Berlin, Heidelberg, 2010, pp. 185–193, https://doi.org/10.1007/978-3-642-15251-1\_15. Lecture Notes in Computer Science.
- [43] C.G. Robertson, N.J. Hardman, Nature of carbon black reinforcement of rubber: perspective on the original polymer nanocomposite, Polymers 13 (4) (2021) 1–28, https://doi.org/10.3390/polym13040538.
- [44] R. Amin, Y.-M. Chiang, Characterization of electronic and ionic transport in Li1-xNi0.33Mn0.33Co0.33O2 (NMC333) and Li1-xNi0.50Mn0.20Co0.30O2 (NMC523) as a function of Li content, J. Electrochem. Soc. 163 (8) (May 2016) A1512, https://doi.org/10.1149/2.0131608jes.
- [45] I. Saadoune, C. Delmas, On the LixNio.8Co0.2O2System, J. Solid State Chem. 136 (1) (Feb. 1998) 8–15, https://doi.org/10.1006/jssc.1997.7599.
- [46] A. Jetybayeva, et al., Unraveling the state of charge-dependent electronic and ionic structure-property relationships in NCM622 cells by multiscale characterization, ACS Appl. Energy Mater. 5 (2) (Feb. 2022) 1731–1742, https://doi.org/10.1021/ acsaem\_103173
- [47] E.M. Dannenberg, Carbon black dispersion and reinforcement, Rubber Chem. Technol. 25 (4) (Dec. 1952) 843–857, https://doi.org/10.5254/1.3543445.
- [48] R.J. Cembrola, The relationship of carbon black dispersion to electrical resistivity and vulcanizate physical properties, Polym. Eng. Sci. 22 (10) (1982) 601–609, https://doi.org/10.1002/pen.760221004.
- [49] E. Hayakawa, H. Nakamura, S. Ohsaki, S. Watano, Dry mixing of cathode composite powder for all-solid-state batteries using a high-shear mixer, Adv. Powder Technol. 33 (8) (Aug. 2022) 103705, https://doi.org/10.1016/j. apt.2022.103705.
- [50] Q.T. Zhou, L. Qu, I. Larson, P.J. Stewart, D.A.V. Morton, Effect of mechanical dry particle coating on the improvement of powder flowability for lactose monohydrate: a model cohesive pharmaceutical powder, Powder Technol. 207 (1–3) (2011) 414–421, https://doi.org/10.1016/j.powtec.2010.11.028.
- [51] W. Haselrieder, et al., Influence of formulation method and related processes on structural, electrical and electrochemical properties of LMS/NCA-blend electrodes, Prog. Solid State Chem. 42 (4) (Dec. 2014) 157–174, https://doi.org/10.1016/j. progsolidstchem 2014 04 009
- [52] R. Habermann, NOBILTA<sup>TM</sup> Solids mixing with high energy intensity, Keram. Z. 59 (4) (2007) 254-259.
- [53] H. Bockholt, W. Haselrieder, A. Kwade, Intensive dry and wet mixing influencing the structural and electrochemical properties of secondary lithium-ion battery cathodes, ECS Trans. 50 (26) (Apr. 2013) 25–35, https://doi.org/10.1149/ 05026.0025ecst.